Chemical Engineering Journal 249 (2014) 102–110

Contents lists available at ScienceDirect

Chemical Engineering Journal

journal homepage: www.elsevier.com/locate/cej

# Designing three-dimensional acicular sheaf shaped $BiVO_4$/reduced graphene oxide composites for efficient sunlight-driven photocatalytic degradation of dye wastewater

Shuying Dong [a], Yanrui Cui [a], Yifei Wang [b], Yukun Li [a], Limin Hu [a], Jingyu Sun [c,*], Jianhui Sun [a,*]

[a] School of Environment, Henan Normal University, Key Laboratory for Yellow River and Huai River Water Environmental and Pollution Control, Ministry of Education, Henan Key Laboratory for Environmental Pollution Control, Xinxiang, Henan 453007, PR China
[b] State Key Laboratory of Water Environment Simulation, School of Environment, Beijing Normal University, Beijing 100875, PR China
[c] Center for Nanochemistry (CNC), College of Chemistry and Molecular Engineering, Peking University, Beijing 100871, PR China

## HIGHLIGHTS

- Designed fabrication of uniform acicular sheaf shaped $BiVO_4$/RGO composites was reported.
- The photocatalytic properties of pure $BiVO_4$ and $BiVO_4$/RGO composites were studied upon sunlight irradiation.
- The mainly active species ($h^+$) involved in the photocatalytic process were probed.
- The cycle-stability of the $BiVO_4$/RGO photocatalysts was examined.

## GRAPHICAL ABSTRACT

Tailored synthesis of uniform 3D acicular sheaf shaped $BiVO_4$/RGO composites is achieved under mild conditions, which exhibit enhanced performances in the photocatalytic degradation of Rhodamine B under natural sunlight irradiation.

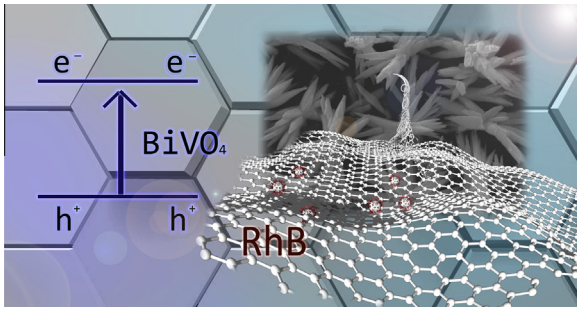


## ARTICLE INFO

*Article history:*
Received 16 December 2013
Received in revised form 13 March 2014
Accepted 20 March 2014
Available online 29 March 2014

*Keywords:*
$BiVO_4$
RGO
Acicular sheaf
Natural sunlight
Photocatalytic

## ABSTRACT

A simple and cost-effective method for the tailored synthesis of uniform three dimensional (3D) acicular sheaf shaped $BiVO_4$ architectures under mild conditions was designed, where the as-synthesized $BiVO_4$ products were then incorporated with prepared reduced graphene oxide (RGO) sheets to form novel $BiVO_4$/RGO composites. The obtained composites were well characterized with the aid of various techniques to study their morphological, physical, optical, and photo-chemical properties. Photocatalytic performances of the pure 3D $BiVO_4$ architectures and $BiVO_4$/RGO composites have been evaluated by investigating the degradation of Rhodamine B-contained wastewater under natural sunlight irradiation, where the $BiVO_4$/RGO composites displayed enhanced sunlight-driven photocatalytic activities. The effects of the active species involved in the photocatalytic process and the cycle-stability of the as-obtained $BiVO_4$/RGO photocatalysts have also been examined.



## 1. Introduction

Water purification is of great significance in alleviating the increasingly serious water resource crisis as well as tackling the

* Corresponding authors. Tel.: +86 10 62757157 (J.Y. Sun). Tel.: +86 373 3325971 (J.H. Sun).
*E-mail addresses:* sunjy-cnc@pku.edu.cn (J.Y. Sun), sunjh@htu.cn (J.H. Sun).

http://dx.doi.org/10.1016/j.cej.2014.03.071
1385-8947/

growing concern over the water contamination. However, conventional water purification methods such as adsorption, flocculation–sedimentation, ion exchange, biological treatment, and filtration, despite their wide usage and popularity, have usually been identified to be inefficient and cost-ineffective, which could lead to the production of secondary pollution [1–5]. In this regard, heterogeneous photocatalysis with its strong oxidation power, moderate operation temperature, and green-chemistry related procedures has by far attracted considerable attention during the past decades, offering a tantalizing route to meet the global challenges associated with the environment, energy and sustainability by virtue of abundant sunlight resources [6]. To date, $TiO_2$ has been broadly employed for various photocatalytic applications due to its non-toxicity, good photocatalytic activity, and high stability under light irradiation [7,8]. However, its activation limited to ultra-violet (UV) light range has substantially impeded the usage of $TiO_2$ in real solar-light photocatalytic circumstances [9]. Therefore, developing photocatalysts which are capable of utilizing visible light photons is indispensable.

Recent years have witnessed a growing interest in using $BiVO_4$ materials with different crystal phases and distinct three-dimensional (3D) morphologies as photocatalysts for the purification of polluted water under sunlight irradiation. $BiVO_4$ with various morphological shapes such as tubes [10], hollow peanuts [11], dumbbells [12], hollow spindles [13], spheres [14], and cages [15] have been synthesized, aiming to better tune the photocatalytic capacities of materials to achieve enhanced performances in pollutant degradation. However, the drawbacks of pure $BiVO_4$ with regard to its poor adsorptive ability and migration difficulty of photo-generated electron–hole pairs have limited its further use in practical applications [16].

Incorporating pure $BiVO_4$ with graphene-related materials (e.g. reduced graphene oxide (RGO)) serves as a reliable route to improve the photocatalytic responses and performances in terms of pollutant degradation. The specifically two-dimensional conjugated structure and uniquely intrinsic properties of graphene (as well as RGO) guarantee its usage as a supporting platform to disperse and stabilize semiconductors for potential applications in catalysis [17–25]. In particular, the integration of $BiVO_4$ and RGO to form novel photocatalytic composites has been of great interest because of the augmentation of photocatalytic activities under visible-light irradiation [26–28]. As abovementioned, $BiVO_4$ materials have been featured by their 3D specific shaped hierarchical architectures, which could bring about a plethora of new properties and applications [29–31]. However, there have been seldom studies [32] exploring the incorporation of 3D hierarchical shaped $BiVO_4$ with RGO for the application in photocatalysis, possibly due to the severe breakage/damage of the original $BiVO_4$ architectures during the synthetic process caused by harsh treatment of samples.

Herein, we design a simple and cost-effective method for the controllable synthesis of uniform 3D acicular sheaf shaped $BiVO_4$ hierarchical structures under mild conditions, which have been further anchored onto the prepared RGO sheets to form $BiVO_4$/RGO composites. The as-synthesized products were well characterized with the aid of X-ray diffraction (XRD), Fourier transform infrared spectroscopy (FT-IR), scanning electron microscopy (SEM), transmission electron microscopy (TEM), $N_2$ adsorption–desorption isotherm, photoluminescence (PL) spectroscopy, UV–visible diffuse reflectance (UV–vis DR) spectroscopy, and Raman spectroscopy. Photocatalytic performances of as-prepared 3D acicular sheaf $BiVO_4$ architectures and $BiVO_4$/RGO composites have been evaluated by investigating the degradation of Rhodamine B (RhB)-contained wastewater under sunlight irradiation, where the $BiVO_4$/RGO composites displayed enhanced sunlight-driven photocatalytic activities.

## 2. Experimental

### 2.1. Synthesis of 3D acicular sheaf shaped $BiVO_4$/RGO ($BiVO_4$/RGO) composites

All the chemicals were analytical grade reagents and used as received without further purification. Deionized water was used throughout this study.

#### 2.1.1. Synthesis of 3D acicular sheaf shaped $BiVO_4$

In a typical synthesis procedure, 0.97 g $Bi(NO_3)_3{\cdot}5H_2O$ was dissolved in a 50 mL mixed solution of $C_2H_5OH$:$CH_3COOH$:$H_2O$ (1:1:3 $v/v/v$) by vigorous stirring for 20 min, the prepared solution was marked as solution A. Meanwhile, 0.23 g $NH_4VO_3$ was dissolved in a 20 mL ammonia solution ($NH_3{\cdot}H_2O$:$H_2O$ 3:1 $v/v$) by vigorous stirring for 20 min, after which the resultant solution was marked as solution B. Then B was added into A at room temperature under continuous stirring for 30 min until it became homogeneous, and the pH value of the mixture was correspondingly adjusted to 7 by using $NH_3{\cdot}H_2O$ or $CH_3COOH$. The obtained mixture was consequently transferred into a Teflon-lined stainless steel autoclave and maintained at 80 °C for 3 h. After the heating, the autoclave was naturally cooled down to room temperature. The yellow precipitate was then collected by filtration, washed by deionized water and ethanol, and dried at 80 °C in an oven overnight to form the desired 3D acicular sheaf shaped $BiVO_4$ architectures.

#### 2.1.2. Synthesis of $BiVO_4$/RGO composites

GO was synthesized from natural graphite powder according to the recipe described in our previous study [24]. To synthesize the $BiVO_4$/RGO composites, a certain amount of GO (with 0.25, 0.5, 1, 1.5, 2, and 3 wt% GO concentration in the final product) was dispersed in 50 mL $H_2O$ with 2 h sonication, followed by adding 1.2 g as-prepared 3D acicular sheaf shaped $BiVO_4$ under gentle stirring for 2 h until it became homogeneous. After adding a small amount of $NH_3{\cdot}H_2O$ and $N_2H_4{\cdot}H_2O$, the suspension was placed into a water bath and maintained at 80 °C for 2 h. After naturally cooling down to room temperature, the composites were processed by filtration, rinsed with water and ethanol for several times, and then dried at 60 °C overnight. The as synthesized $BiVO_4$/RGO composites with 0.25, 0.5, 1, 1.5, 2, and 3 wt% RGO concentrations were labeled as BG-0.25, BG-0.5, BG-1, BG-1.5, BG-2, and BG-3, respectively. The color of the synthesized composites by naked-eye observation was changed from yellow to dark green as the RGO concentration (wt%) increased from 0.25% to 3%.

### 2.2. Characterizations

The crystal phase of the prepared 3D acicular sheaf shaped $BiVO_4$ hierarchical structures was analyzed by X-ray diffraction (XRD). The patterns were recorded in the $2\theta$ range of 10–70° with a scan rate of 0.02°/0.4 s using a Bruker-D8-AXS diffractometer system equipped with a Cu K$\alpha$ radiation ($\lambda$ = 0.15406 Å) (Bruker Co., Germany). The morphologies of obtained materials were inspected by using a JSM-6390LV scanning electron microscopy (SEM) and a JEM-2100 transmission electron microscopy (TEM). Fourier transform infrared (FT-IR) spectra were recorded using a FTIR Analyzer (Perkin–Elmer, Spectrum 400), and the KBr was used to serve as a reference. The measurements of low-temperature $N_2$ adsorption were carried out by using a Micromeritics ASAP 2020 apparatus operating at −196 °C, where all the samples were degassed at 100 °C for 6 h prior to the measurement. The ultraviolet–visible diffuse reflectance (UV–vis DR) spectra were obtained with the aid of a UV–Vis–NIR spectrophotometer (Lambda 950, PerkinElmer) by using $BaSO_4$ as a reference, where the spectra were

recorded at the wavelength range of 300–800 nm. The photoluminescence (PL) spectra of samples were recorded using a Fluorescence Spectrophotometer (FP-6500, Japan) equipped with a Xenon lamp at an excitation wavelength of 325 nm. The Raman spectra were acquired on a Horiba LabRAM HR-800 Raman spectroscopy using a 514 nm laser wavelength.

### 2.3. Evaluation of sunlight photocatalytic activity

The photocatalytic activities of the as-obtained products were monitored through the photo-degradation of RhB under natural sunlight irradiation. Photocatalytic reactions were carried out in a 250 mL borosilicate photochemical batch reactor. To ensure the sufficient illumination of the natural sunlight, all photocatalytic experiments were intentionally performed between 8:10 a.m. and 6:10 p.m. (the reaction time was 10 h) on those sunny days during the September 2013 at Xinxiang, Henan Province, China. The ambient temperature was between 20 °C and 26 °C, where the illumination was estimated to be at approx. 8000–66,000 lux. In all experiments, the as-synthesized photocatalyst (0.10 g) were added to 200 mL RhB aqueous solution (5 mg $L^{-1}$). No pH adjustment was used during the entire course of the photo-degradation process. Prior to irradiation, the suspension was magnetically stirred (300 rpm) in the dark for 40 min, in order to achieve an adsorption–desorption equilibrium between the RhB molecules and catalyst particles. During each photocatalytic experiment, 2 mL of the suspension was collected at predesigned time intervals for analysis.

The concentration of RhB was analyzed by measuring the absorption intensity at its maximum absorbance wavelength of $\lambda$ = 553 nm using a UV–vis spectrophotometer (UV-1700, SHIMADU) with a 1 cm path length spectrometric quartz cell, and was calculated from the calibration curve. The degradation efficiency of the RhB dye wastewater was determined according to the following equation:

$$\text{Degradation efficiency } (\%) = \frac{C_0 - C_t}{C_0} \times 100\% \quad (1)$$

where $C_0$ was the initial concentration of RhB (after the standing in the dark for 40 min) and $C_t$ was the concentration of RhB at certain reaction time $t$ (h).

### 2.4. Evaluation of simulated sunlight photocatalytic activity

Several offset photocatalytic tests were carried out through the photo-degradation of RhB solution (with a concentration of 10 mg $L^{-1}$) under simulated sunlight irradiation. A 300 W U-shaped xenon lamp was used as the light source (Yaming Company, Shanghai) and the irradiation time was 60 min. The temperature of the reactions was maintained at room temperature with the aid of a water circulation system. The other experimental apparatus and procedures employed were identical to that described in Section 2.3.

## 3. Results and discussion

### 3.1. Detailed characterizations of the as-synthesized photocatalysts

XRD was employed to characterize the crystal phases of 3D acicular sheaf shaped $BiVO_4$ architectures and $BiVO_4$/RGO composites, the patterns of which are shown in Fig. 1. It is found that all the samples present the typical XRD diffraction character of monoclinic scheelite $BiVO_4$ phase (International Center for Diffraction Data, JCPDS No. 14-0688), confirming the crystalline nature of obtained samples. However, it is worth-noting that no typical diffraction peaks of RGO ($2\theta$ = 26° and 44°) are observed within the

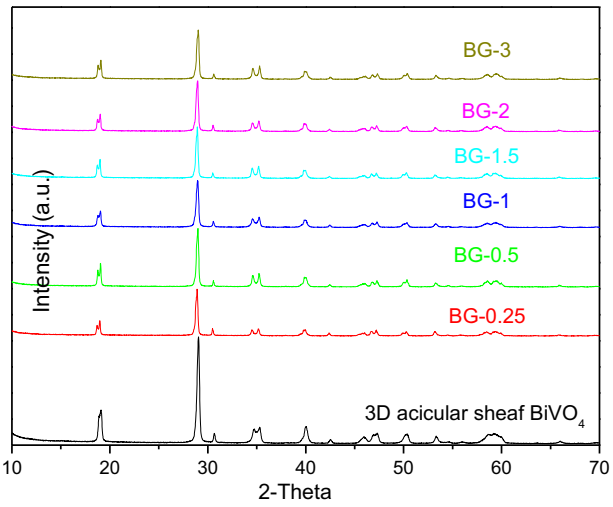


**Fig. 1.** XRD patterns of as-synthesized 3D acicular sheaf shaped $BiVO_4$ architectures and $BiVO_4$/RGO composites.

$BiVO_4$/RGO composites, which may be due to the fact that the relatively small dosage amount and low diffraction intensity of RGO in the composite [33]. Furthermore, the diffraction intensity of $BiVO_4$/RGO composite is weaker than the pure $BiVO_4$ architectures, indicating the imperfect crystallinity occurred when dosing RGO in the synthetic process.

FT-IR spectra of GO, 3D acicular sheaf shaped $BiVO_4$ architectures and $BiVO_4$/RGO composites are shown in Fig. 2. In the spectrum of GO (black curve), the broad band at 3412 $cm^{-1}$ (black curve) are assigned to O—H stretching vibrations of adsorbed water molecules on GO [34]. Several characteristic bands at approx. 1065, 1219, 1404, 1625, and 1724 $cm^{-1}$ are attributed to the stretching vibration of C—O—C, stretching mode of C—OH, the O—H deformation within the C—OH group, the C=C stretching mode, and the C=O stretching vibrations within the —COOH group, respectively. Compared to the spectrum of GO, the bands featuring oxygen-containing functional groups almost vanish in the spectrum of all the $BiVO_4$/RGO composites, indicating the successful and effective reduction of GO sheets. Moreover, the bands at 730 $cm^{-1}$ for both the samples of 3D $BiVO_4$ and $BiVO_4$/RGO composites are associated with the bending vibration of the $VO_4^{3-}$ [35].

Fig. 3 shows the representative SEM micrographs of the as-synthesized 3D acicular sheaf shaped $BiVO_4$ architectures and $BiVO_4$/RGO composites. In terms of the top-view SEM observations of the 3D $BiVO_4$ (Fig. 3a and b), it can be seen that the obtained pure $BiVO_4$ are of uniform size and shape distributions. The individual particle possesses acicular sheaf shaped architecture, probably formed *via* assembly of a series of needle-like structures. The sizes of these 3D shaped particles falling into micron scale range have allowed us to map out the size distributions based on the analysis of the SEM micrographs. Fig. 3c and d shows the histograms of the particle length distribution and aspect ratio (length to width) distribution of as-synthesized 3D acicular sheaf shaped $BiVO_4$ architectures, respectively, with the inset in Fig. 3d indicates the definition of the length ($l$) and width ($w$) of an individual structure. Both distribution histograms clearly indicate that the as-synthesized 3D $BiVO_4$ architectures are of uniform size distributions. Fig. 3e and f displays the SEM observation of the $BiVO_4$/RGO composites, where stratiform RGO sheets (marked by red[1] circles in Fig. 3e) can be observed despite the low dosages.

[1] For interpretation of color in Figs. 3, 8 and 9, the reader is referred to the web version of this article.

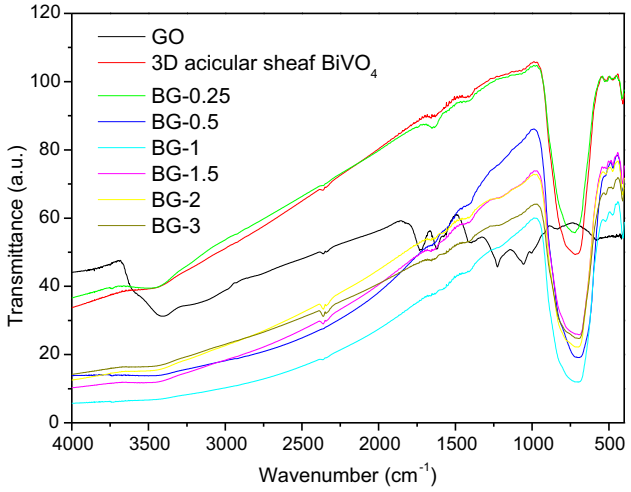


**Fig. 2.** FT-IR spectra of as-prepared GO, 3D acicular sheaf shaped $BiVO_4$ architectures, and $BiVO_4$/RGO composites (with different RGO loadings).

Fig. 4 displays the TEM characterization of the prepared 3D $BiVO_4$ (Fig. 4a and b) and $BiVO_4$/RGO composites (Fig. 4c and d), where detailed morphological information of synthesized materials can be obtained. The representative TEM images in Fig. 4a and b confirms the prepared $BiVO_4$ are of uniformly 3D acicular sheaf shapes. The low and high magnified TEM observations in Fig. 4c and d show the typical wrinkles of RGO sheets, which are freely coated on the surface of 3D $BiVO_4$, confirming the formation of $BiVO_4$/RGO composites. The incorporated RGO sheets seem not detached or damaged during TEM sample preparation (sonication), indicating the stability of both the 3D $BiVO_4$ architectures and $BiVO_4$/RGO composites.

It is well-realized that the separation of photo-generated electrons and holes is one of the most important factors affecting the photocatalytic activities of a photocatalyst. The photoluminescence (PL) measurement is a facile technique to study the photochemical properties of semiconductor materials, where the PL emission mainly originates from the recombination of the excited electrons and holes [11]. Also, it has been reported that a higher PL peak intensity corresponded to a greater probability of charge

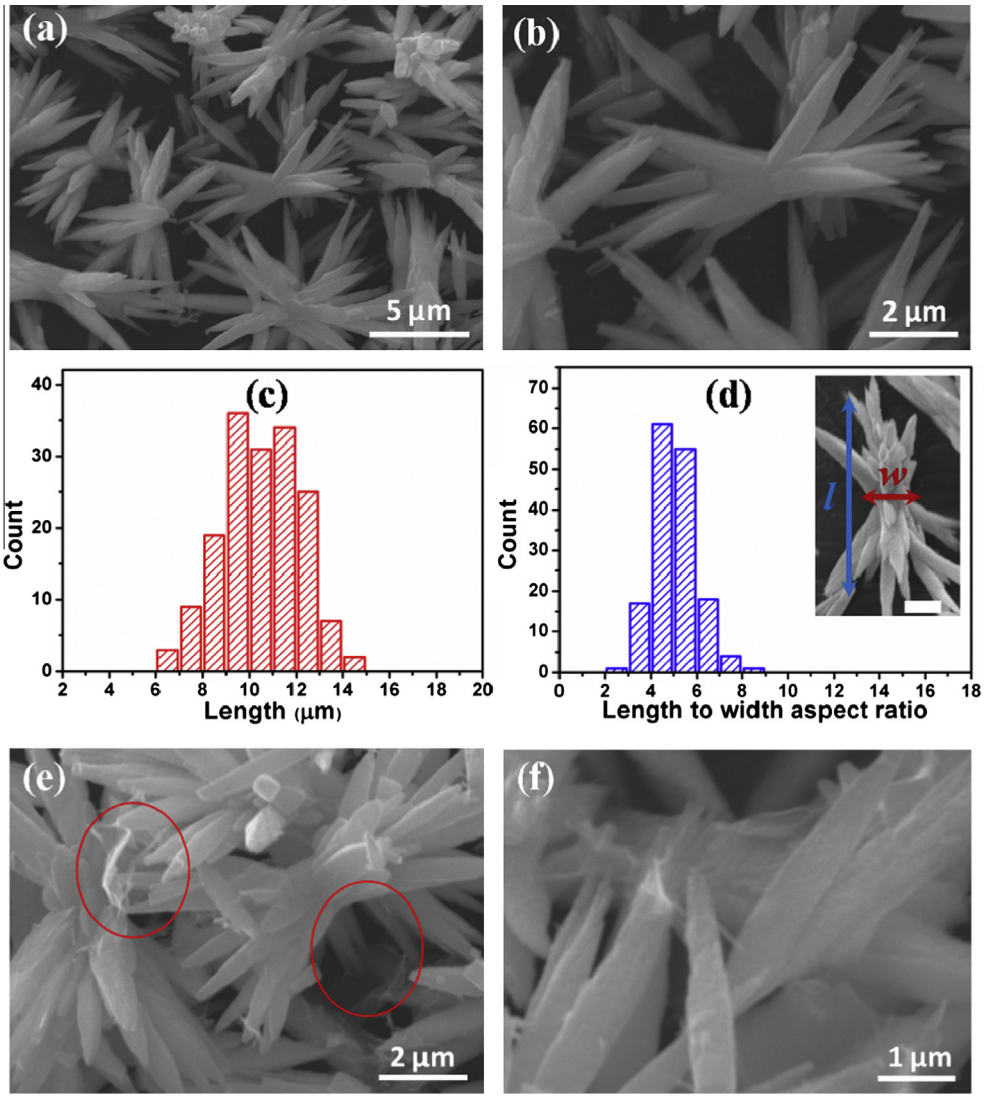


**Fig. 3.** SEM images of the prepared 3D acicular sheaf shaped $BiVO_4$ (a and b), statistical histograms of the length distribution (c) and aspect ratio distribution (d) of the 3D $BiVO_4$ products, and SEM images of BG-1 composites (e and f). The inset in (d) shows an SEM image displaying the denotation of the length ($l$) and width ($w$) of an individual $BiVO_4$ architecture. Scale bar: 2 μm.

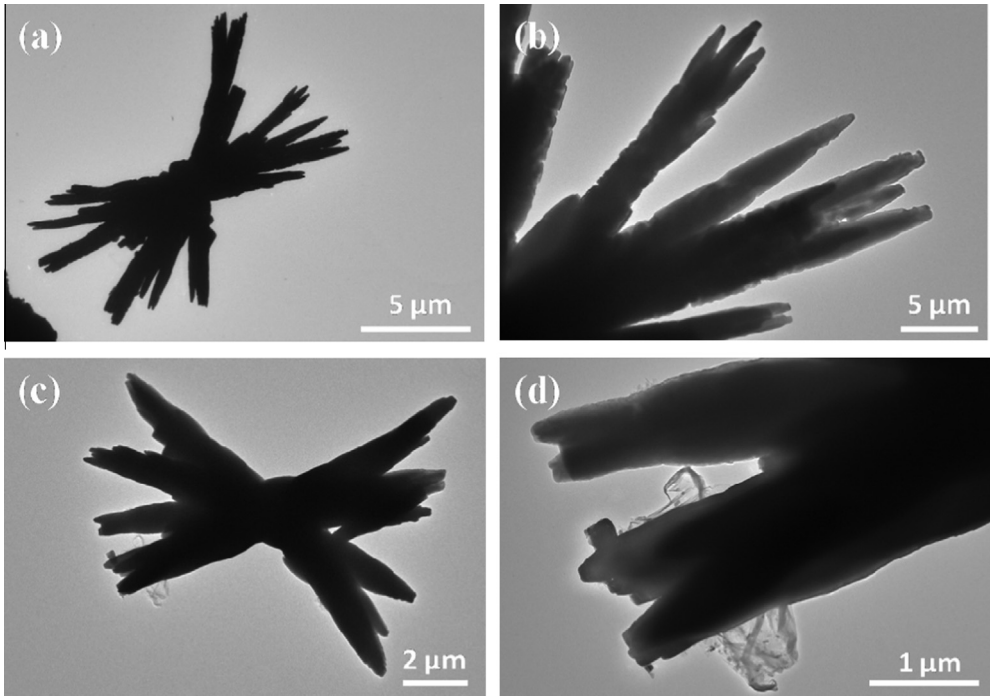


**Fig. 4.** The HRTEM images of the as-prepared 3D acicular sheaf shaped $BiVO_4$ architectures (a and b) and BG-1 composites (c and d).

carrier recombination [36]. Fig. 5 shows the PL spectra of the as-synthesized 3D acicular sheaf shaped $BiVO_4$ architectures and $BiVO_4$/RGO composites. All the samples possess strong PL peaks centering at approx. 525 nm. By comparing the spectra of pure $BiVO_4$ architectures and $BiVO_4$/RGO composites, one can observe that the PL emission intensities of all the $BiVO_4$/RGO composites stay weaker than that of pure $BiVO_4$, the reason of which might be attributed to an efficient charge separation achieved by direct electron transfer from the $BiVO_4$ to the RGO *via* the chemical bonding of Bi—V—O—C within the composites. Previous study has indicated that the RGO could act as an electron transfer channel in the RGO-incorporated semiconductor composites, where it aided in maintaining a lower rate of electron–hole recombination, leading to maximized charge separations thus enhanced photocatalytic activities [37]. Our finding is consistent with the results reported in previous work, suggesting that RGO might improve the photocatalytic activity of 3D acicular sheaf shaped $BiVO_4$ architectures.

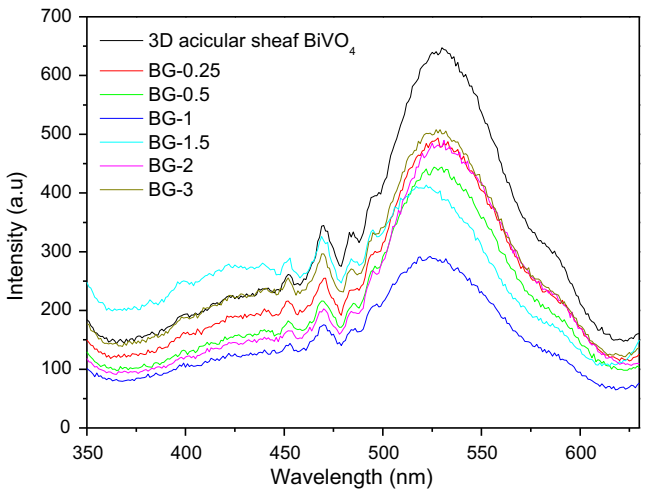


**Fig. 5.** PL spectra of the as-synthesized 3D acicular sheaf shaped $BiVO_4$ architectures and $BiVO_4$/RGO composites.

The optical absorption property of the semiconductor has been recognized as the key factor in affecting its photocatalytic performance [38]. Fig. 6a shows the UV–vis DR spectra of the as-synthesized 3D acicular sheaf shaped $BiVO_4$ architectures and $BiVO_4$/RGO composites. The 3D $BiVO_4$ exhibits a strong absorption in the UV light region but an almost vanished absorption signal in visible light region. However, all the $BiVO_4$/RGO composite samples with different RGO dosages exhibit strong absorption characters in the whole range. The steep shapes of the spectra indicate that the visible-light absorption is not due to the transition from impurity levels but the band-gap transition. The better performance in the light absorption in the visible light range by the $BiVO_4$/RGO composites could lead to its enhanced sunlight-driven photocatalytic activities for the degradation of RhB-contained wastewater. It is worth-noting that the absorption edges for $BiVO_4$/RGO composites red-shift compared with that of pure $BiVO_4$, where the absorption edge has been measured to be at approx. 530 nm (3D $BiVO_4$), 552 nm (BG-0.25), 556 nm (BG-0.5), 558 nm (BG-1), 560 nm (BG-1.5), 562 nm (BG-2), and 572 nm (BG-3), respectively, indicating that the incorporation of RGO could affect the photo-adsorption properties of the photocatalyst [39]. Moreover, the energy band structures of a semiconductor stay important in determining its photocatalytic activity. The relationship of absorbance and incident photon energy $h\nu$ can be described by Eq. (2).

$$Ah\nu = C(h\nu - E_g)^{1/2} \tag{2}$$

where $A$, $E_g$, $h$, and $\nu$ represent the absorption coefficient, the band-gap energy, Planck constant, and the incident light frequency, respectively, and $C$ denotes a constant. The band-gap energy ($E_g$) of the obtained photocatalysts can therefore be estimated from a plot depicting $(Ah\nu)^2$ versus $h\nu$. The intercept of the tangent to the $x$ axis gives rise to a good approximation of the band-gap energy for the 3D acicular sheaf shaped $BiVO_4$ architectures and $BiVO_4$/RGO composites (Fig. 6b). The estimated band-gap energies of 3D $BiVO_4$ architectures and $BiVO_4$/RGO composites have been measured to be approx. 2.46 eV (3D $BiVO_4$), 2.36 eV (BG-0.25), 2.35 eV (BG-0.5), 2.34 eV (BG-1), 2.33 eV (BG-1.5), 2.32 eV (BG-2) and 2.28 eV (BG-3), respectively.

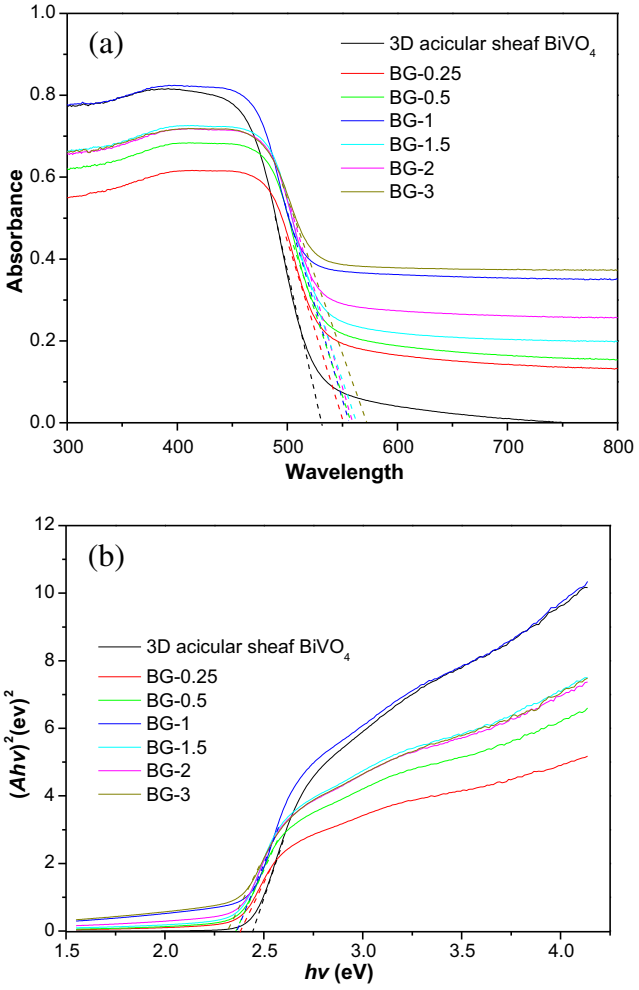


**Fig. 6.** (a) UV–vis DR spectra and (b) the relationship between $(Ahv)^2$ and the photon energy ($hv$) of the as-synthesized 3D acicular sheaf shaped $BiVO_4$ architectures and $BiVO_4$/RGO composites.

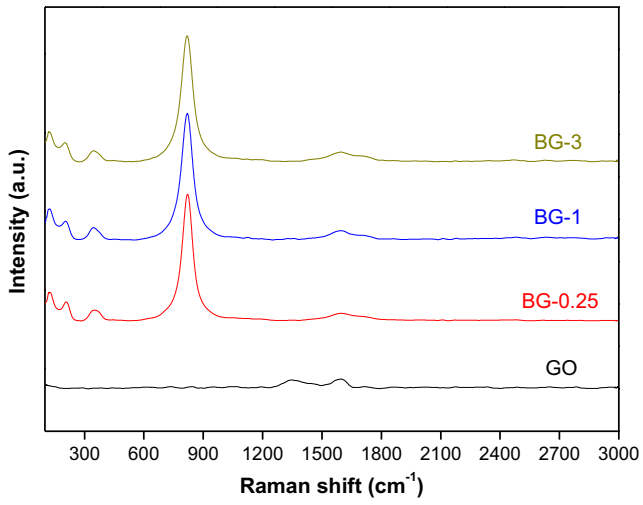


**Fig. 7.** Raman spectra of the as-synthesized graphene oxide (GO) and $BiVO_4$/RGO composites.

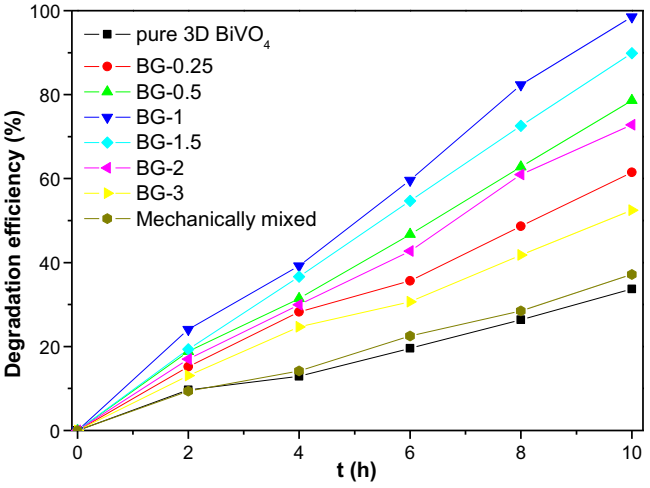


**Fig. 8.** The comparison of the degradation efficiencies of RhB (5 mg $L^{-1}$) in aqueous solution by using pure 3D acicular sheaf shaped $BiVO_4$ architectures and $BiVO_4$/RGO composites as photocatalysts under natural sunlight irradiation.

Raman spectroscopy serves as one of the most helpful tools to characterize the carbon-based materials. Fig. 7 shows the Raman spectra of GO and selective RGO–$BiVO_4$ composites (BG-0.25, BG-1, and BG-3). The reported Raman spectrum of GO is featured with a D-band shift at 1360 $cm^{-1}$ and a G-band shift at 1597 $cm^{-1}$ [40], both of which is presented in the black curve in Fig. 7. However, the D-band shift of GO is fully suppressed in the Raman spectra of all three composite samples, whilst the G-band shift is replaced by a broad shift peak. This phenomenon is consistent with that observed in the microwave-assisted *in situ* preparation of RGO–$BiVO_4$ composites [28], where the D/G ratio close to zero suggested the effective reduction of GO to RGO.

### 3.2. Photocatalytic activities and recycle performances

#### 3.2.1. Investigating the photocatalytic activity of the 3D $BiVO_4$ architectures and $BiVO_4$/RGO composites

The photocatalytic activities of the as-prepared 3D acicular sheaf shaped $BiVO_4$ architectures and $BiVO_4$/RGO composites with different RGO loadings were evaluated towards RhB degradation under sunlight irradiation. To eliminate the adsorption of dye molecules by the photocatalysts, dark adsorption tests were performed. The results shown in Fig. S1 indicate that after the adsorption–desorption equilibrium (40 min) between the RhB molecules and catalyst particles, no obvious loss of RhB can be detected afterwards even that the dark tests were prolonged to 2 h. Fig. 8 shows the degradation efficiency of RhB in aqueous solution by using as-prepared 3D acicular sheaf shaped $BiVO_4$ architectures and $BiVO_4$/RGO composites. For comparison, in the absence of photocatalyst, the sunlight photolysis of 5 mg $L^{-1}$ RhB aqueous solution was tested. It was found that no significant changes of the concentration of RhB occurred after 10 h irradiation (data not shown), indicating that RhB was not prone to degradation by sunlight photolysis. With the presence of photocatalysts, the degradation efficiency of RhB reaches 33.7% after 10 h sunlight irradiation only by pure $BiVO_4$ (black curve in Fig. 8). In contrast, $BiVO_4$/RGO composites (BG-1) display a much greater photo-degradation performance, where the corresponding degradation efficiency achieves 98.5% under the identical conditions (blue curve in Fig. 8). Moreover, it is revealed in Fig. 8 that the photocatalytic activities of the composites increase with the increase of the RGO loading from 0.25 wt% to 1 wt%, however, further increase of the RGO contents results in a decrease of the photocatalytic activities. For instance, when RGO dosage is 2 wt%, an apparent decrease in the degradation efficiency can be observed (pink curve in Fig. 8). This is probably due to the fact that high RGO loading prevents the $BiVO_4$ from absorbing light [20]. Our surface area

measurements of these composites prior to the photocatalytic evaluations indicate a trend that the surface area of samples increases with the growing dosages of RGO (1.6758 $m^2 g^{-1}$ for pure $BiVO_4$, 1.8023 $m^2 g^{-1}$ for BG-0.25, 3.6215 $m^2 g^{-1}$ for BG-0.5, 6.1261 $m^2 g^{-1}$ for BG-1, 8.216 $m^2 g^{-1}$ for BG-1.5, 11.0995 $m^2 g^{-1}$ for BG-2, and 12.676 $m^2 g^{-1}$ for BG-3, respectively). Hence our results herein reveal that the surface areas of the composites did not play a dominant role in the enhancement of photocatalytic activities when incorporating RGO with $BiVO_4$. Besides, our results are in agreement with those reported in previous studies, in which suitable RGO content was crucial for optimizing the photocatalytic performance of the $BiVO_4$/RGO composites [28,32]. Furthermore, control experiment regarding the evaluation of the photocatalytic performance of mechanically mixed sample (mechanical mixture of $BiVO_4$ and 1 wt% RGO) was performed, where the sample exhibits far lower degradation efficiency than those of normally-treated $BiVO_4$/RGO composites (light-brown curve in Fig. 8), suggesting that a proper route to integrating RGO with $BiVO_4$ is of great importance.

With respect to selecting RhB as the target pollutant for photodegradation investigations, RhB-contained aqueous solution with an RhB concentration of 5 or 10 mg $L^{-1}$ has standardizingly been employed [41–43]. Min et al. [41] reported the comparison study of the photocatalytic activities between pure $Bi_5Nb_3O_{15}$ and $Bi_5Nb_3O_{15}$/graphene *via* photocatalytic decolorization of RhB (with a concentration of 5 mg $L^{-1}$) under visible light irradiation. Martínez-Orozco et al. [42] evaluated the photocatalytic activity of Ag/GO nanocomposites throughout the photocatalytic degradation of RhB with a concentration of 10 mg $L^{-1}$. In our case, to fully probe the advanced photocatalytic capacities of the $BiVO_4$/RGO composites, further investigation (Fig. 9) on photocatalytic performances was concerned with visible light degradation of RhB-contained (10 mg $L^{-1}$) solutions by using prepared samples, namely, pure RGO, 3D $BiVO_4$ architectures, 3D $BiVO_4$ architectures treated by $N_2H_4{\cdot}H_2O$, $BiVO_4$/RGO composites (BG-1), and $BiVO_4$–RGO physical mixtures, where the values of surface areas of the last two samples were controlled to be the same, aiming to eliminate potential reason of photocatalytic activity associated with just the surface area increase of RGO. It can be clearly seen from Fig. 9 that, in the presence of only pure RGO or pure 3D $BiVO_4$, the degradation efficiency is only about 10% (blue curve in Fig. 9) and 42.6% (magenta curve in Fig. 9), respectively, whilst a complete removal of RhB can be achieved by employing BG-1 within 60 min irradiation time (navy-blue curve in Fig. 9).

The degradation experiment by 3D $BiVO_4$ architectures treated by $N_2H_4{\cdot}H_2O$ was conducted to exclude the side-effect regarding the involvement of $N_2H_4{\cdot}H_2O$ on enhancing the photocatalytic activity. As shown by the green curve in Fig. 9, after 60 min visible light irradiation, the degradation efficiency of RhB only reaches approx. 44.2%, almost identical to that of pure $BiVO_4$ (42.6%), indicating that treating $BiVO_4$ with $N_2H_4{\cdot}H_2O$ in the synthetic stage exerted no influence on the correspondingly photocatalytic activity in the current study. It is also noted from Fig. 9 that, under visible light irradiation (duration: 60 min), the degradation efficiency of RhB with the involvement of $BiVO_4$–RGO physical mixtures reaches only 51.3% (red curve in Fig. 9), which demonstrates that the mere increase of surface area from RGO during the synthesis of BG-1 might not be one of the potential reasons accounting for the improvement of their photocatalytic activity. Moreover, the present study indicates that the light absorption efficiency within the composites in the presence of RGO improves, meanwhile, the charge recombination rate decreases substantially. According to one of our latest report [32], it can be speculated that the superior visible-light-driven photocatalytic activity of the $BiVO_4$/RGO composites might be attributed to the enhanced light harvesting efficiency and reduced charge recombination rates.

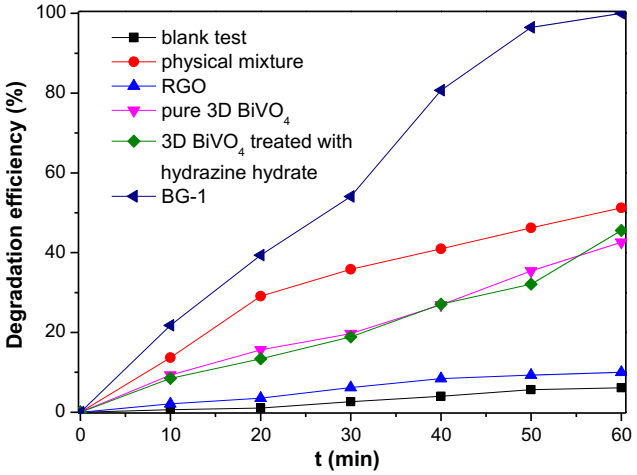


**Fig. 9.** The comparison of the degradation efficiencies of RhB (10 mg $L^{-1}$) in aqueous solution by testing different species as photocatalysts under sunlight irradiation, highlighting the enhanced photocatalytic performances of BG-1 composites.

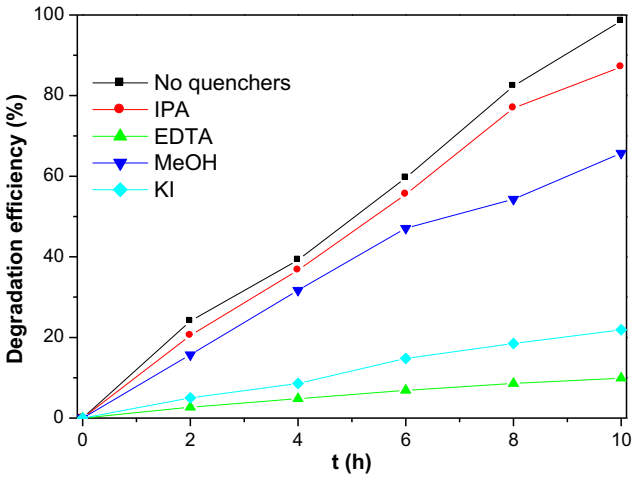


**Fig. 10.** Trapping experiments of photocatalytic degradation of RhB over the BG-1 composites under natural sunlight irradiation with/without the presence of quenchers.

### *3.2.2. Probing the main oxidative species in terms of natural sunlight-driven degradation of RhB by $BiVO_4$/RGO composites*

It is of paramount importance to detect main active species in the photocatalytic reaction for elucidating the photocatalytic mechanism of synthesized $BiVO_4$/RGO composites, where the detection can be realized through trapping experiments of oxidative species such as ·OH, $h^+$, and $\cdot O_2^-$ by using isopropanol (IPA) (·OH scavenger), ethylene diamine tetraacetic acid (EDTA) ($h^+$ scavenger), methyl alcohol (MeOH) ($\cdot O_2^-$ scavenger), and potassium iodide (KI) (·OH and $h^+$ scavenger) respectively. The control experiments were performed without quenchers under identical conditions. The result in terms of RhB degradation efficiency over the BG-1 sample using different quenchers is shown in Fig. 10. It can be observed that IPA or MeOH has little influence on the RhB degradation, indicating that ·OH and $\cdot O_2^-$ radicals on the surface of the $BiVO_4$/RGO composites do not play a major role in the photocatalytic system. However, the photocatalytic activity of BG-1 can be greatly suppressed by the addition of an $h^+$ scavenger (EDTA), suggesting that the photo-generated holes are the dominant oxidative species of $BiVO_4$/RGO composites, where the ·OH and $\cdot O_2^-$ radicals play an assistant role in the natural sunlight-driven degradation of RhB.

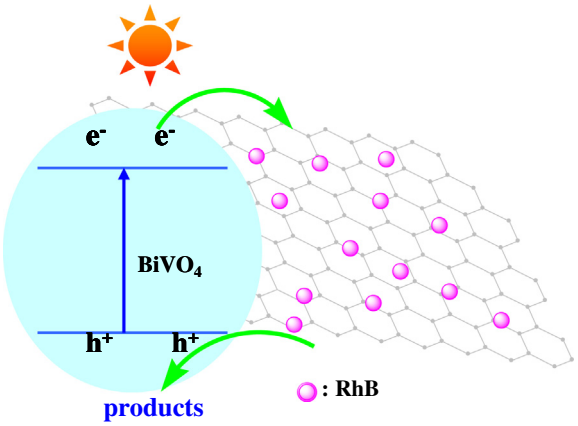


**Scheme 1.** Speculated illustration for the photocatalytic degradation of RhB under natural sunlight irradiation over fabricated $BiVO_4$/RGO composites.

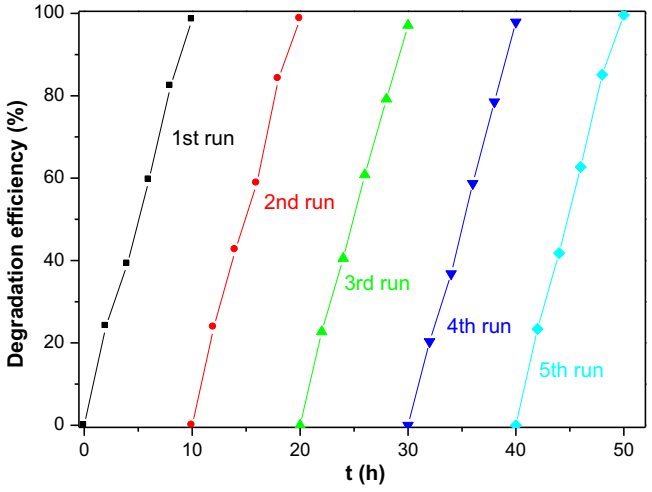


**Fig. 11.** Photo-stability tests over the BG-1 composites for the cycling photodegradation of RhB under natural sunlight irradiation.

Base on the above investigation, a possible mechanism for the photocatalytic degradation of RhB over $BiVO_4$/RGO composites can be proposed (Scheme 1). Under the sunlight irradiation, the reaction starts with the activation of the $BiVO_4$/RGO composites, resulting in the promotion of electrons ($e^-$) from the valence band (VB) to the conduction band (CB) of the $BiVO_4$ catalysts and the generation of holes ($h^+$) in the VB. RhB molecules adsorbed on the surface of $BiVO_4$ are directly oxidized by $h^+$, besides, $h^+$ also have few opportunity to react with $OH^-/H_2O$ to form ·OH radicals, and the photo-generated $e^-$ in the CB of the $BiVO_4$ can be injected into RGO, therefore hindering the recombination process of the $e^-$–$h^+$ pairs and leading to an effective charge separation and stabilization. On the other hand, $e^-$ could transport along the RGO sheets from inner region to the surface and react with $O_2$ to form $\cdot O_2^-$ radicals, although $\cdot O_2^-$ radical is not efficient in the degradation of aromatic compounds such as RhB molecules [44].

*3.2.3. Testing the recycle performances of $BiVO_4$/RGO composites*

The recycle experiments were performed to evaluate the photocatalytic repeatability and stability of as-synthesized $BiVO_4$/RGO composites under sunlight irradiation. The BG-1 samples can be easily recycled by a simple sedimentation without further treatment. As shown in Fig. 11, after five cycling runs of photodegradation of RhB (at the duration of 10 h for each cycle), the photocatalytic capacity of $BiVO_4$/RGO composites has not exhibited any significant loss. Moreover, the BG-1 samples employed in the recycle tests were further characterized by SEM and FTIR after the experiments. The corresponding SEM micrograph (Fig. 12a) and FT-IR spectrum (Fig. 12b) reveal that there is no observable change in the morphological shapes as well as the crystal structures of the photocatalysts. These results indicate that the prepared $BiVO_4$/RGO composites possess excellent stability and are not prone to suffering from photo-corrosion during the degradation process.

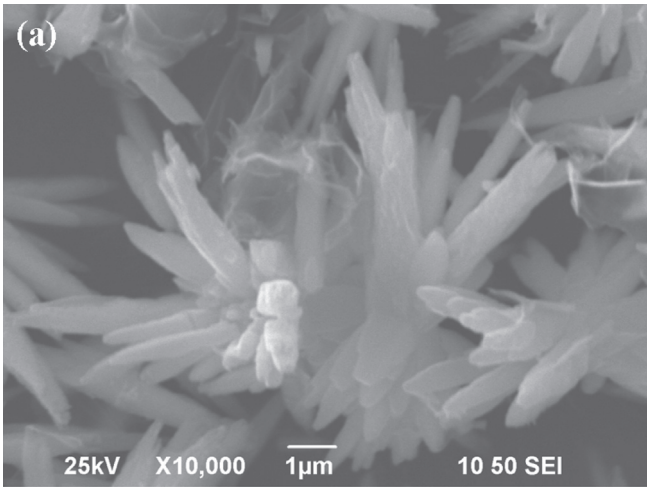


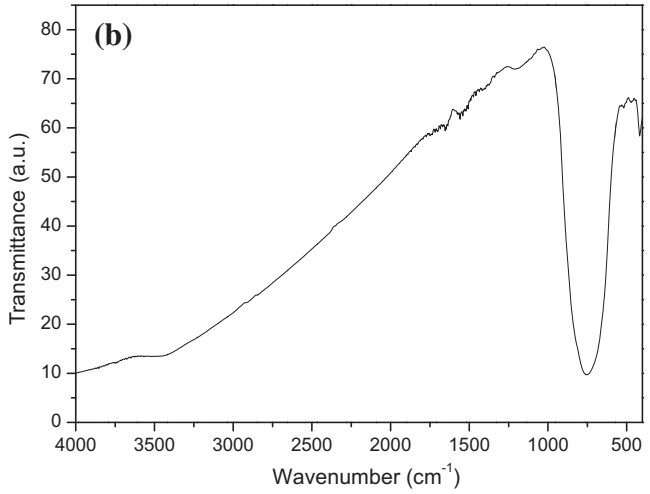


**Fig. 12.** Characterization of BG-1 composites after the recycle experiment showing SEM micrograph (a) and FT-IR spectrum (b).

## 4. Conclusions

To sum up, we designed a simple and low-cost method for the controllable synthesis of uniform 3D acicular sheaf shaped $BiVO_4$/RGO composites under gentle conditions, where the as-synthesized $BiVO_4$/RGO composites exhibited far greater photocatalytic performances towards the degradation of RhB in the aqueous solution. The improvement in the photocatalytic activity when incorporating RGO with 3D acicular sheaf shaped $BiVO_4$ could be attributed to the unique morphological structure, enhanced light harvesting efficiency and reduced charge recombination rate of the composites. Furthermore, the as-prepared $BiVO_4$/RGO composites possess good photocatalytic repeatability and stability over prolonged irradiation time. Our present work suggests that integrating RGO with unique shaped semiconductors might offer special insights into designing novel hybrid photocatalysts for addressing broader water-pollution issues.

## Acknowledgements

The authors are grateful for the financial support from the Basic Scientific and Technological Frontier Project of Henan Province, PR China (Grant Nos. 132330410138, 102300410098, and 122300410293), the Key Science and Technology Program of Henan Province, PR China (Grant Nos. 122102310486 and 132102210129). The authors also would like to thank the Innovation Scientists and Technicians Troop Construction Projects of Henan Province, the Plan for Scientific Innovation Talent of Henan Province (Grant No. 134200510014), and the Fostering Foundation of Henan Normal University for the Author of National Excellent Ph.D. Dissertation, PR China (Grant No. 01333900011).

## Appendix A. Supplementary material

Supplementary material associated with this article can be found, in the online version, at http://dx.doi.org/10.1016/j.cej.2014.03.071.

## References

[1] N.M. Mubarak, J.N. Sahu, E.C. Abdullah, N.S. Jayakumar, Removal of heavy metals from wastewater using carbon nanotubes, Sep. Purif. Rev. 43 (2014) 311–338.
[2] C. Wang, C. Shang, G. Chen, X. Zhu, Mechanisms of nC60 removal by the alum coagulation–flocculation–sedimentation process, J. Colloid Interface Sci. 411 (2013) 213–219.
[3] K.A. Landry, T.H. Boyer, Diclofenac removal in urine using strong-base anion exchange polymer resins, Water Res. 47 (2013) 6432–6444.
[4] D. Krzeminska, E. Neczaj, K. Parkitna, Application of Fenton reaction for supporting biological wastewater treatment from the dairy industry, Rocz. Ochr. Sr. 15 (2013) 2381–2397.
[5] E.J. Park, H.J. Jo, H.J. Kim, K. Cho, J. Jung, Effects of gamma-ray treatment on wastewater toxicity from a rubber products factory, J. Radioanal. Nucl. Chem. 277 (2008) 619–624.
[6] X. Zhang, X. Quan, S. Chen, H. Yu, Constructing graphene/$InNbO_4$ composite with excellent adsorptivity and charge separation performance for enhanced visible-light-driven photocatalytic ability, Appl. Catal. B: Environ. 105 (2011) 237–242.
[7] S.L. Cao, K.L. Yeung, P.L. Yue, Preparation of freestanding and crack-free titania–silica aerogels and their performance for gas phase, photocatalytic oxidation of VOCs, Appl. Catal. B: Environ. 68 (2006) 99–108.
[8] S.L. Cao, K.L. Yeung, P.L. Yue, An investigation of trichloroethylene photocatalytic oxidation on mesoporous titania–silica aerogel catalysts, Appl. Catal. B: Environ. 76 (2007) 64–72.
[9] H. Jiang, H. Dai, X. Meng, L. Zhang, J. Deng, K. Ji, Morphology-dependent photocatalytic performance of monoclinic $BiVO_4$ for methyl orange degradation under visible-light irradiation, Chin. J. Catal. 32 (2011) 939–949.
[10] Y. Sun, B. Qu, Q. Liu, S. Gao, Z. Yan, W. Yan, B. Pan, S. Wei, Y. Xie, Highly efficient visible-light-driven photocatalytic activities in synthetic ordered monoclinic $BiVO_4$ quantum tubes–graphene nanocomposites, Nanoscale 4 (2012) 3761–3767.
[11] L. Chen, S.-F. Yin, R. Huang, Q. Zhang, S.-L. Luo, C.-T. Au, Hollow peanut-like m-$BiVO_4$: facile synthesis and solar-light-induced photocatalytic property, CrystEngComm. 14 (2012) 4217–4222.
[12] S. Obregón, A. Caballero, G. Colón, Hydrothermal synthesis of $BiVO_4$: structural and morphological influence on the photocatalytic activity, Appl. Catal. B: Environ. 117–118 (2012) 59–66.
[13] W. Liu, L. Cao, G. Su, H. Liu, X. Wang, L. Zhang, Ultrasound assisted synthesis of monoclinic structured spindle $BiVO_4$ particles with hollow structure and its photocatalytic property, Ultrason. Sonochem. 17 (2010) 669–674.
[14] H.Q. Jiang, H. Endo, H. Natori, M. Nagai, K. Kobayashi, Fabrication and photoactivities of spherical-shaped $BiVO_4$ photocatalysts through solution combustion synthesis method, J. Eur. Ceram. Soc. 28 (2008) 2955–2962.
[15] Z. Zhu, J. Du, J. Li, Y. Zhang, D. Liu, An EDTA-assisted hydrothermal synthesis of $BiVO_4$ hollow microspheres and their evolution into nanocages, Ceram. Int. 38 (2012) 4827–4834.
[16] H.Q. Jiang, H. Endo, H. Natori, M. Nagai, K. Kobayashi, Fabrication and efficient photocatalytic degradation of methylene blue over CuO/$BiVO_4$ composite under visible-light irradiation, Mater. Res. Bull. 44 (2009) 700–706.
[17] Y. Zhang, Y. Zhu, J. Yu, D. Yang, T.W. Ng, P.K. Wong, J.C. Yu, Enhanced photocatalytic water disinfection properties of $Bi_2MoO_6$–RGO nanocomposites under visible light irradiation, Nanoscale 5 (2013) 6307–6310.
[18] Q. Xiang, J. Yu, M. Jaroniec, Graphene-based semiconductor photocatalysts, Chem. Soc. Rev. 41 (2012) 782–796.
[19] S. Yin, Y. Zhang, J. Kong, C. Zou, C.M. Li, X. Lu, J. Ma, F.Y.C. Boey, X. Chen, Assembly of graphene sheets into hierarchical structures for high-performance energy storage, ACS Nano 5 (2011) 3831–3838.
[20] P. Madhusudan, J. Yu, W. Wang, B. Cheng, G. Liu, Facile synthesis of novel hierarchical graphene–$Bi_2O_2CO_3$ composites with enhanced photocatalytic performance under visible light, Dalton Trans. 41 (2012) 14345–14353.
[21] M. Khenfouch, M. Baïtoul, M. Maaza, White photoluminescence from a grown ZnO nanorods/graphene hybrid nanostructure, Opt. Mater. 34 (2012) 1320–1326.
[22] W. Wang, J. Yu, Q. Xiang, B. Cheng, Enhanced photocatalytic activity of hierarchical macro/mesoporous $TiO_2$–graphene composites for photodegradation of acetone in air, Appl. Catal. B: Environ. 119 (2012) 109–116.
[23] F. Yavari, M.A. Rafiee, J. Rafiee, Z.Z. Yu, N. Koratkar, Dramatic increase in fatigue life in hierarchical graphene composites, ACS Appl. Mater. Interfaces 2 (2010) 2738–2743.
[24] S.Y. Dong, J.Y. Sun, Y.K. Li, C.F. Yu, Y.H. Li, J.H. Sun, $ZnSnO_3$ hollow nanospheres/reduced graphene oxide nanocomposites as high-performance photocatalysts for degradation of metronidazole, Appl. Catal. B: Environ. 144 (2014) 386–393.
[25] S.Y. Dong, Y.K. Li, J.Y. Sun, C.F. Yu, Y.H. Li, J.H. Sun, Facile synthesis of novel ZnO/RGO hybrid nanocomposites with enhanced catalytic performance for visible-light-driven photodegradation of metronidazole, Mater. Chem. Phys. 145 (2014) 357–365.
[26] Y.H. Ng, A. Iwase, A. Kudo, R. Amal, Reducing graphene oxide on a visible-light $BiVO_4$ photocatalyst for an enhanced photoelectrochemical water splitting, J. Phys. Chem. Lett. 1 (2010) 2607–2612.
[27] Y.S. Fu, X.Q. Sun, X. Wang, $BiVO_4$–graphene catalyst and its high photocatalytic performance under visible light irradiation, Mater. Chem. Phys. 131 (2011) 325–330.
[28] Y. Yan, S. Sun, Y. Song, X. Yan, W. Guan, X. Liu, W. Shi, Microwave-assisted in situ synthesis of reduced graphene oxide–$BiVO_4$ composite photocatalysts and their enhanced photocatalytic performance for the degradation of ciprofloxacin, J. Hazard. Mater. 250 (2013) 106–114.
[29] M. Shang, W. Wang, J. Ren, S. Sun, L. Zhang, A novel $BiVO_4$ hierarchical nanostructure: controllable synthesis, growth mechanism, and application in photocatalysis, CrystEngComm. 12 (2010) 1754–1758.
[30] G. Tan, L. Zhang, H. Ren, S. Wei, J. Huang, A. Xia, Effects of pH on the hierarchical structures and photocatalytic performance of $BiVO_4$ powders prepared via the microwave hydrothermal method, ACS Appl. Mater. Interfaces 5 (2013) 5186–5193.
[31] S.Y. Dong, J.L. Feng, Y.K. Li, L.M. Hu, M.L. Liu, Y.F. Wang, Y.Q. Pi, J.Y. Sun, J.H. Sun, Shape-controlled synthesis of $BiVO_4$ hierarchical structures with unique natural-sunlight-driven photocatalytic activity, Appl. Catal. B: Environ. 152–153 (2014) 413–424.
[32] Y.K. Li, S.Y. Dong, Y.F. Wang, J.Y. Sun, Y.F. Li, Y.Q. Pi, L.M. Hu, J.H. Sun, Reduced graphene oxide on a dumbbell-shaped $BiVO_4$ photocatalyst for an augmented natural sunlight photocatalytic activity, J. Mol. Catal. A: Chem. 387 (2014) 138–146.
[33] D. Fu, G. Han, Y. Chang, J. Dong, The synthesis and properties of ZnO–graphene nano hybrid for photodegradation of organic pollutant in water, Mater. Chem. Phys. 132 (2012) 673–681.
[34] H. Hu, X. Wang, F. Liu, J. Wang, C. Xu, Rapid microwave-assisted synthesis of graphene nanosheets–zinc sulfide nanocomposites: optical and photocatalytic properties, Synth. Met. 161 (2011) 404–410.
[35] M. Gotic, S. Music, M. Ivanda, M. Soufek, S. Popovic, Synthesis and characterisation of bismuth vanadate, J. Mol. Struct. 744 (2005) 535–540.
[36] L. Chen, Q. Zhang, R. Huang, S.-F. Yin, S.-L. Luo, C.-T. Au, Porous peanut-like $Bi_2O_3$–$BiVO_4$ composites with heterojunctions: one-step synthesis and their photocatalytic properties, Dalton Trans. 41 (2012) 9513–9518.
[37] Y.-L. Min, K. Zhang, Y.-C. Chen, Y.-G. Zhang, Enhanced photocatalytic performance of $Bi_2WO_6$ by graphene supporter as charge transfer channel, Sep. Purif. Technol. 86 (2012) 98–105.
[38] S. Chen, W. Zhao, W. Liu, S. Zhang, Preparation, characterization and activity evaluation of p–n junction photocatalyst p-ZnO/n-$TiO_2$, Appl. Surf. Sci. 255 (2008) 2478–2484.
[39] J. Zhang, J. Yu, M. Jaroniec, J.R. Gong, Noble metal-free reduced graphene oxide–$Zn_xCd_{1-x}S$ nanocomposite with enhanced solar photocatalytic $H_2$-production performance, Nano Lett. 12 (2012) 4584–4589.
[40] S. Stankovich, D.A. Dikin, R.D. Piner, K.A. Kohlhaas, A. Kleinhammes, Y.Y. Jia, Y. Wu, S.T. Nguyen, R.S. Ruoff, Synthesis of graphene-based nanosheets via chemical reduction of exfoliated graphite oxide, Carbon 45 (2007) 1558–1565.
[41] Y. Min, F.-J. Zhang, W. Zhao, F. Zheng, Y. Chen, Y. Zhang, Hydrothermal synthesis of nanosized bismuth niobate and enhanced photocatalytic activity by coupling of graphene sheets, Chem. Eng. J. 209 (2012) 215–222.
[42] R.D. Martínez-Orozco, H.C. Rosu, S.-W. Lee, V. Rodríguez-González, Understanding the adsorptive and photoactivity properties of Ag–graphene oxide nanocomposites, J. Hazard. Mater. 263 (2013) 52–60.
[43] P. Wang, J. Xian, J. Chen, Y. He, J. Wang, W. Li, Y. Shao, D. Li, Preparation, photocatalytic activity, and mechanism of $Cd_2Sb_2O_{6.8}$–graphene composite, Appl. Catal. B: Environ. 144 (2014) 644–653.
[44] L. Ye, X. Liu, Q. Zhao, H. Xie, L. Zan, Dramatic visible light photocatalytic activity of $MnO_x$–BiOI heterogeneous photocatalysts and the selectivity of the cocatalyst, J. Mater. Chem. 1 (2013) 8978–8983.